LA-UR-17-20721 (Accepted Manuscript)

Strain fields induced by kink band propagation in Cu-Nb nanolaminate composites

Nizolek, Thomas Joseph
Begley, Matthew R
Mccabe, Rodney James
Avallone, Jaclyn T.
Mara, Nathan Allan
Beyerlein, Irene Jane
Pollock, Tresa M.

To be published in: Acta Materialia

DOI to publisher's version: 10.1016/j.actamat.2017.04.050

Permalink to record: http://permalink.lanl.gov/object/view?what=info:lanl-repo/lareport/LA-UR-17-20721

Accepted Manuscript

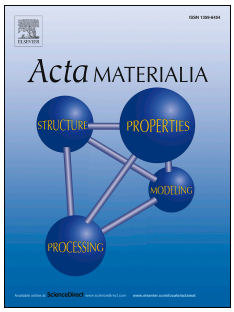

Strain fields induced by kink band propagation in Cu-Nb nanolaminate composites

T.J. Nizolek, M.R. Begley, R.J. McCabe, J.T. Avallone, N.A. Mara, I.J. Beyerlein, T.M. Pollock

PII: S1359-6454(17)30342-7

DOI: 10.1016/j.actamat.2017.04.050

Reference: AM 13737

To appear in: *Acta Materialia*

Received Date: 6 February 2017

Revised Date: 18 April 2017

Accepted Date: 23 April 2017

Please cite this article as: T.J. Nizolek, M.R. Begley, R.J. McCabe, J.T. Avallone, N.A. Mara, I.J. Beyerlein, T.M. Pollock, Strain fields induced by kink band propagation in Cu-Nb nanolaminate composites, *Acta Materialia* (2017), doi: 10.1016/j.actamat.2017.04.050.

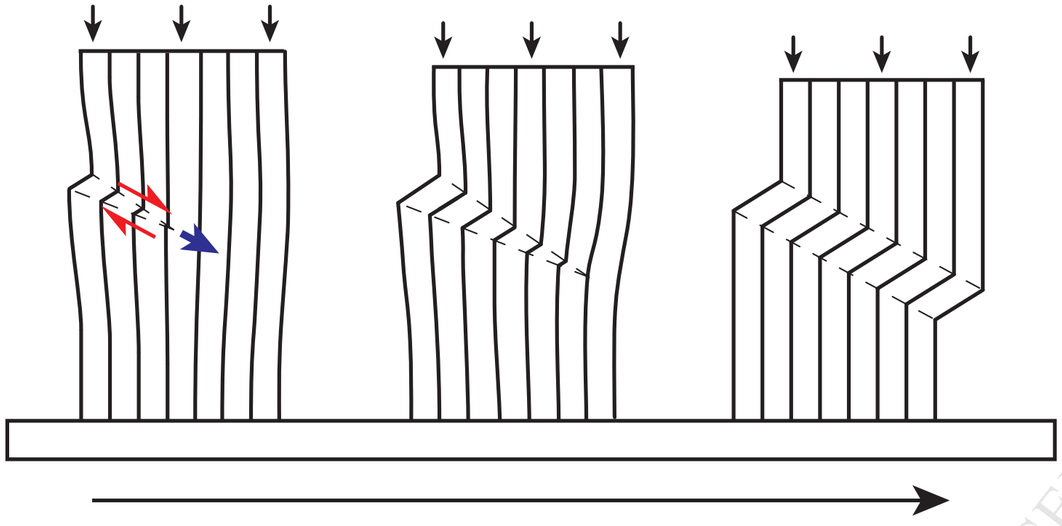

Kink band formation via nucleation and propagation

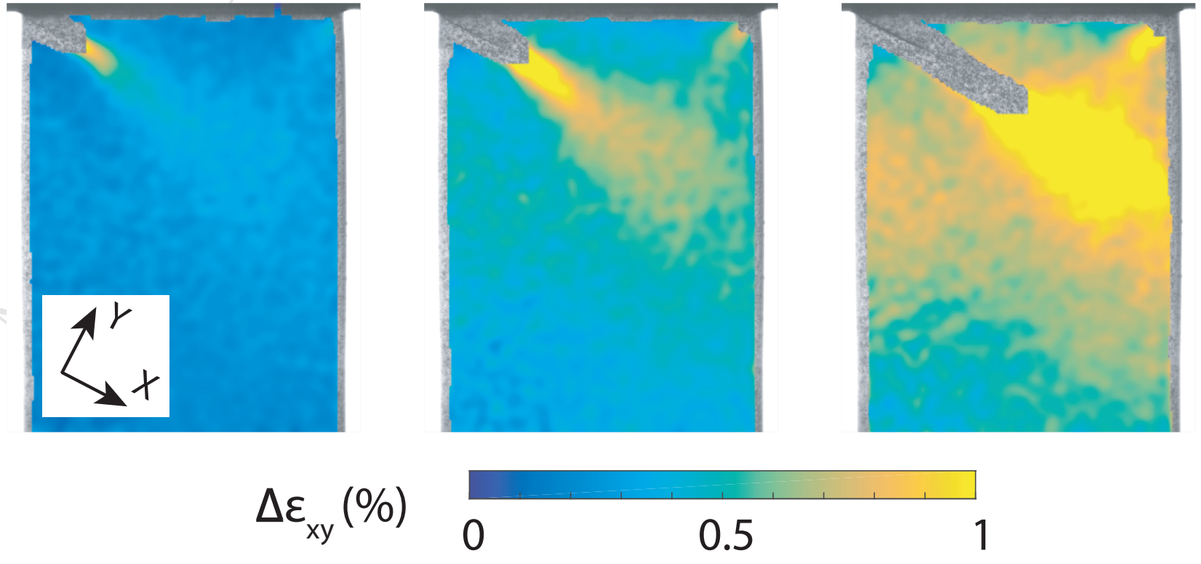

Kink band propagation strain fields obtained *via* DIC

Strain fields induced by kink band propagation in Cu-Nb nanolaminate composites

T.J. Nizolek[a,*], M.R. Begley[a], R.J. McCabe[b], J.T. Avallone[a], N.A. Mara[c], I.J. Beyerlein[a], T.M. Pollock[a]

[a] *University of California Santa Barbara, Santa Barbara, CA, 93106, USA*
[b] *MST-8, Los Alamos National Laboratory, Los Alamos, NM 87545, USA*
[c] *Institute for Materials Science and the Center for Integrated Nanotechnologies, Los Alamos National Laboratory, Los Alamos, NM 87545, USA*

Abstract

Kink band formation is a common deformation mode for anisotropic materials and has been observed in polymer matrix fiber composites, single crystals, geological formations, and recently in metallic nanolaminates. While numerous studies have been devoted to kink band formation, the majority do not consider the often rapid and unstable process of kink band propagation. Here we take advantage of stable kink band formation in Cu-Nb nanolaminates to quantitatively map the local strain fields surrounding a propagating kink band during uniaxial compression. Kink bands are observed to initiate at specimen edges, propagate across the sample during a rising global stress, and induce extended strain fields in the non-kinked material surrounding the propagating kink band. It is proposed that these stress/strain fields significantly contribute to the total energy dissipated during kinking and, analogous to crack tip stress/strain fields, influence the direction of kink propagation and therefore the kink band inclination angle.

Keywords: kink band, digital image correlation, anisotropy, multilayers, deformation band

1. Introduction

Kink band formation is a type of strain localization that has been observed in a multitude of anisotropic single phase and composite materials. While significant attention has been given to kink band formation in fiber composites due to the technological importance of these materials [1–3], kink bands have also been observed in oriented polymers [4], geological and mineral samples [5, 6], biological materials such as wood and abalone shell [8, 9], and low symmetry single crystals such as cadmium, ceramic ternary carbide 'MAX'

*Corresponding author
Email address: tnizolek@lanl.gov (T.J. Nizolek)

phases, and freshwater ice [10–12]. Despite the broad range of material classes and constitutive behaviors, the observed deformation bands possess common features that warrant the use of the general term 'kink band.' A kink band can be defined by the following characteristics: 1) the deformation band consists of a region that is either microstructurally or crystallographically misoriented from the rest of the sample, 2) the angle of misorientation (ϕ) is approximately uniform across the width of the band, and 3) there exists a specific relationship between the boundary of the deformation band and the rotation of the material within the deformation band such that the boundary nominally bisects the angle made between the deformed and undeformed material ($\phi = 2\beta$ as shown in Figure 1(a)). This definition excludes other types of deformation bands such as shear bands, compaction bands, and slip bands. While defining a kink band based on these three morphological characteristics is appealing in that it does not place restrictions on the kinematics or deformation processes of kink band formation (which may vary among material classes), a definition based solely on morphology would necessarily include deformation twins as a type of kink band. Twins are not generally considered kink bands, although the striking geometric similarities have been discussed [13] and can be seen in Figure 1(a) (where the lines shown would correspond to the conjugate K_2 twin planes). While twins, from a continuum mechanics perspective, could be considered to be a special subset of kink bands where the magnitude of shear is prescribed by the need to preserve the crystallographic structure, convention dictates that twins should be excluded. This requires the addition of a fourth criterion for kink bands: 4) the plane of the kink band boundary must not be restricted to a specific crystallographic plane.

A common feature of all materials which form kink bands is pronounced mechanical anisotropy. Specifically, the material must possess a set of planes along which the shear strength is very low. For example, in unidirectional fiber or layered composites the necessary anisotropy for kink band formation occurs due to the architecture of the composite; shear on a plane parallel to the fibers or layers requires a much lower stress than shear along any other direction due to the lower strength of the matrix phase [1, 14]. In single phase materials which form kink bands, such as low symmetry single crystals, the anisotropy is inherent to the material, with the planes of low shear strength being the (often single set of) crystallographic slip planes on which dislocation glide readily occurs [15, 16].

When the material is oriented so that the planes of low shear strength are nominally parallel to a compressive stress, a region or band of the material containing slightly misoriented fibers or layers may yield due to layer-parallel shear during compression. Due to the constraint imposed by the surrounding material, this shear induces a rotation, increasing the resolved shear stress in the misoriented region (Figure 1(b)). The resultant geometric softening produced by shear and rotation creates a localized band of misoriented mate-

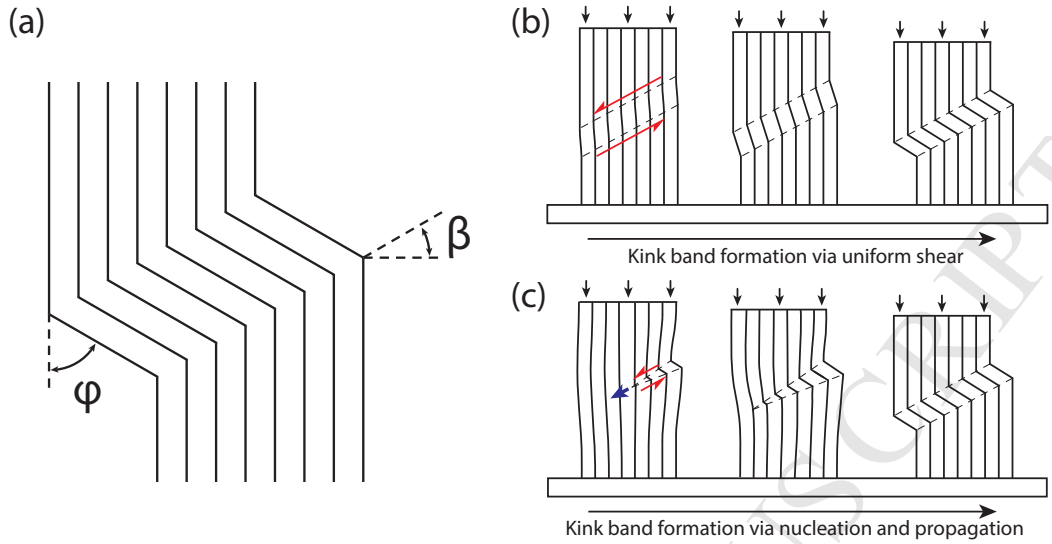

Figure 1: (a) Schematic illustrating the morphology of a kink band showing the $\phi = 2\beta$ relationship. The kinked sample can be envisioned to form via the uniform shearing of a band of material (b) or by an initiation and propagation sequence (c). While the final deformed state may be nearly identical, (c) induces accommodation strains and stress concentration during propagation not present in (b).

rial. The band 'locks up' after a certain amount of rotation (at $\phi = 2\beta$, Figure 1(a)), with further specimen compression being accommodated either by additional kink band formation or by broadening of the original kink band [3, 14].

The question of what limits the deformation within a kink band (why shear and rotation past the $\phi = 2\beta$ relationship is unfavored) has been considered by a variety of researchers. When layer continuity across the kink band boundary is maintained, as depicted in Figure 1(b), the geometry of the band requires that the layer spacing or layer thickness in the kinked material change as a function of rotation angle (ϕ). This layer transverse strain within the kink band increases during shear and rotation from $\phi = 0$ to $\phi = \beta$ and decreases as the material rotates from $\phi = \beta$ to $\phi = 2\beta$. At $\phi = 2\beta$, the layer spacing both inside of and outside of the kink band is identical and the layer transverse strain is zero. According to Paterson and Wiess [5], the significance of the $\phi = 2\beta$ relationship and its implications in terms of layer transverse strain was first noted in 1898 by Mügge [7] who wrote 'In all cases where the kinked parts are not completely separated, the kink plane bisects the angle of the kink [$\phi = 2\beta$]; for since here volume changes of the crystal and also distortion and change in spacing are precluded...' [5]. Stated more concisely, the transverse strain associated with the

rotation of the layers within a kink band returns to zero when $\phi = 2\beta$.

For many materials that form kink bands, such as fiber composites, significant strains parallel to the fibers/layers are precluded by the high stiffness of one of the phases. For fiber composites, the fiber transverse strains required during kinking occur without significant fiber parallel strains and thus the deformation within the kink band is non-isochoric [14]. For these materials, the argument for kink band lock up is based on volume preservation: while dilatation during rotation from $\phi = 0$ to $\phi = \beta$ is accommodated by fiber-matrix delamination and void formation, rotation from $\phi = \beta$ to $\phi = 2\beta$ closes these delaminations and further rotation past $\phi = 2\beta$ is strongly resisted due to material incompressibility. While it should be noted that this explanation requires that that one phase remain inextensible and that delamination occurs to accommodate dilatation, it has been widely accepted for composite materials [2, 24, 30, 31]. An interesting alternative explanation was proposed by Wadee [28] who demonstrated that the $\phi = 2\beta$ relationship could be accounted for, even in the absence of delamination or void formation, by considering the effects of interlamellar friction in transversely compressible stacks of paper. While Wadee's model is only applicable to transversely compressible materials subject to a hydrostatic stress during kinking, the model demonstrates that the $\phi = 2\beta$ relationship may arise through a more subtle interplay of kinematics and constitutive behavior than previously considered.

Most theoretical and experimental studies have focused exclusively on the deformation occurring within the kink band. If a kink band forms by uniform shear across the entire specimen as shown in Figure 1(b), the kink band is the only region that experiences significant deformation; the material on either side of the kink band undergoes only a rigid translation during formation of the kink band. However, significant experimental evidence suggests that kink bands often, if not exclusively, form by initiation at a stress concentration followed by propagation across the sample (Figure 1(c)) [3, 4, 14, 18–23]. The propagation stage is evident provided that the specimen is large relative to the width of the kink band. The occurrence of kink band propagation was recognized early on: Chaplin, in a 1977 study of kinking in glass reinforced polymers, stated 'Anyone who has watched a compression test on a material which demonstrates this compression crease [kinking] type failure be it fibre reinforced composite, wood or some other natural material, will have noticed that it does not fail simultaneously across the section. The failure starts in one region and propagates, often very rapidly, across the sample' [24]. The propagation of kink bands in oriented polyethylene was recorded during in situ tests as early as 1969 [4] yet, presumably due the experimental difficulties of working with high strength fiber composites, similar results were not published in composites literature until decades later [18–22].

While the deformation (shear and rotation to $\phi = 2\beta$) within a propagating kink band (Figure 1(c)) may be nearly identical to that proposed in models that assume uniform kink band formation (Figure 1(b)), the deformation of the specimen surrounding a propagating kink band is markedly different. Compatibility between the kinked and non-kinked material (continuity of fibers or layers) geometrically requires distortion of the material surrounding the kink band. In a semi-infinite specimen, the material remains undistorted far in advance of the kink band tip, while behind the kink band tip the specimen is displaced parallel to the kink band by an amount proportional to the width of the kink band and the uniform shear strain within the kink band. This gradient in displacements naturally requires an accommodation strain field in the material surrounding the kink band. Additionally, stress concentration at the kink band tip leads to local strain fields extending in advance of the kink band that are analogous to crack tip strain fields. The presence of these distortions has been noted by observing fiber bending near the tip of a propagating kink band [4, 18]. However, only limited quantitative measures of the extent or magnitude of these strain fields have been provided. An early study [25] used speckle interferometry to map displacements surrounding a kink band in a carbon fiber/PEEK composite, yet no further analysis was reported. A more recent investigation [26] used digital image correlation (DIC) strain mapping during kink band formation in glass fiber epoxy composites and showed unloading behind the propagating kink band. Unfortunately the large size of the kink band compared to the specimen size did not permit careful study of strain fields at the kink band tip. Kink band propagation was shown more clearly in a 2010 DIC study of failure modes during off-axis compression of unidirectional carbon-epoxy composites [23], however the focus of that investigation was the construction of a failure envelope and therefore the details of kink band propagation were not analyzed.

The local strain and stress fields in the material surrounding a propagating kink band have not been considered in modeling efforts, yet they are important in that they clearly contribute to the total work of kink band formation and likely influence the direction of kink band propagation. Previous investigators have attempted to explain why certain kink band inclination angles (β in Figure 1(a)) should be preferred by considering the effects of pre-existing defects or by considering only the deformation within the kink band [14, 27–30]. Budiansky [27] proposed that β was controlled by the elastic effects of preexisting local imperfections, while Wadee [28] invoked non-isochoric deformation (during multiaxial loading of paper stacks) and proposed that β was set by the layer transverse compressibility. Several investigators [14, 29, 30] have assumed or derived a relationship between β and ϕ and suggest that β evolves through band boundary rotation as the material within the kink band shears. The question of what determines the angle β has proved difficult to answer, with Budiansky concluding that prospects for ‘a simple theoretical criteria for

β based only on analysis of final, uniform, kinked states are not promising' [31]. The difficulty that has been encountered in efforts to predict β may be attributed to the lack of attention that has been paid to the propagation stage of kink band formation. During kink band propagation, the interaction of the stress fields driven by compatibility, as well as those arising from the stress concentration at the tip of a kink band, with the anisotropic composite material should be expected to influence the kink band propagation direction. By identifying the factors that influence the propagation direction, and recognizing that the propagation direction determines the boundary angle of the fully formed kink band, an alternative explanation for what sets β may be found.

Kink bands are the dominant deformation mechanism for Cu-Nb nanolaminates with layer thicknesses below 100 nm when these metal-metal composites are compressed parallel to the layer orientation [32, 33]. Several features make these materials attractive for the study of kink band formation: 1) the load drops associated with kinking are small relative to the high stresses at which kink bands initiate, suggesting stable or near stable growth, 2) layer debonding during kink band formation is infrequent, and 3) the layer length scale and therefore minimum kink band length scale is orders of magnitude smaller than the specimen size. This facilitates in situ observations of kink band propagation and allows for high resolution DIC strain mapping of any strain fields surrounding a narrow, propagating, kink band.

2. Experimental

2.1. Materials and specimens

Cu-Nb nanolaminates were synthesized using the accumulative roll bonding process (ARB). This process creates approximately 4 mm thick sheets of laminate material through an iterative sequence of bonding, rolling, and stacking described in detail in References [33–35]. The material used in the present study contains continuous, alternating, and equal thickness layers of Cu and Nb with a nominal individual layer thickness of 30 nm (see Figure 2(a,b)). While the microstructure evolution during ARB processing is complex, many aspects including crystallographic texture development [34, 36], layer size distributions [35], and interface crystallography [37] have been addressed in the literature and are of limited relevance to the general phenomena of kink band formation in lamellar composites. Noteworthy however is that the resultant material is fully dense and well bonded, displaying a low work hardening rate and appreciable plasticity in both tension and compression (7% and >25% respectively) [35, 38]. While phase resolved mechanical property data has not been obtained for the specific Cu-Nb nanolaminates used in this investigation, nanoindentation

techniques have shown that the Cu and Nb phases have significantly different hardnesses in ARB composites with a 24 μm layer thickness [49]. This nanoindentation data, as well as crystal plasticity modeling [49], suggests that the initial flow stress of the Cu phase is approximately 20% lower than that of the Nb phase in micron-scale Cu-Nb composites

A low temperature annealing step, 400°C for 30 minutes, was conducted after ARB in order to improve the resistance to delamination during layer-parallel compression. When delamination is largely suppressed, the dominant deformation mechanism during layer parallel compression is kink banding (Figure 2(c)) [32, 33]. Figure 2(d) shows a complicated network of kink bands in a 15 nm layer thickness compression specimen, containing kink band intersections and terminations. The complexity of the strain localization shown in Figure 2(d) suggests that kink bands in Cu-Nb laminates form via propagation across a sample as opposed to the uniform band formation process shown in Figure 1(b).

Compression specimens measuring 7.2 mm x 3.6 mm x 3.6 mm were machined from the rolled and annealed laminate plate using wire electric discharge machining. The specimens were carefully aligned with with respect to the layer orientation, with the compression axis (longest dimension) parallel to the transverse direction of the rolled material. Potential damage from the machining operation was removed on four of the six specimen faces via metallographic polishing, with the top and bottom surfaces left in the as machined condition to prevent edge rounding or loss of parallelism. A speckle pattern was applied to one face of the specimens using HP LaserJet 96A toner ink that was fused to the polished surface via brief exposure to a heat lamp.

2.2. Mechanical testing and in-situ imaging

Compression testing was conducted on an MTS servo-hydraulic load frame under displacement control at an initial strain rate of $10^{-4}s^{-1}$. Due to the small specimen size, the need to position specimens centrally on the compression platens, and the lighting requirements of digital image correlation, truncated pyramidal hardened steel pedestals were attached to the compression platens. This allowed for in situ imaging of the compression specimens without reflections or shadowing from the large compression platens. A molybdenum disulfide lubricant was applied between the specimens and the compression pedestals to minimize friction.

A laser extensometer (Electronic Instrument Research model LE-01) was used to measure the distance between two retro-reflective tapes attached to the compression pedestals while local strains on the specimen face were obtained from digital image correlation. The DIC setup consisted of a Point Grey Grasshopper

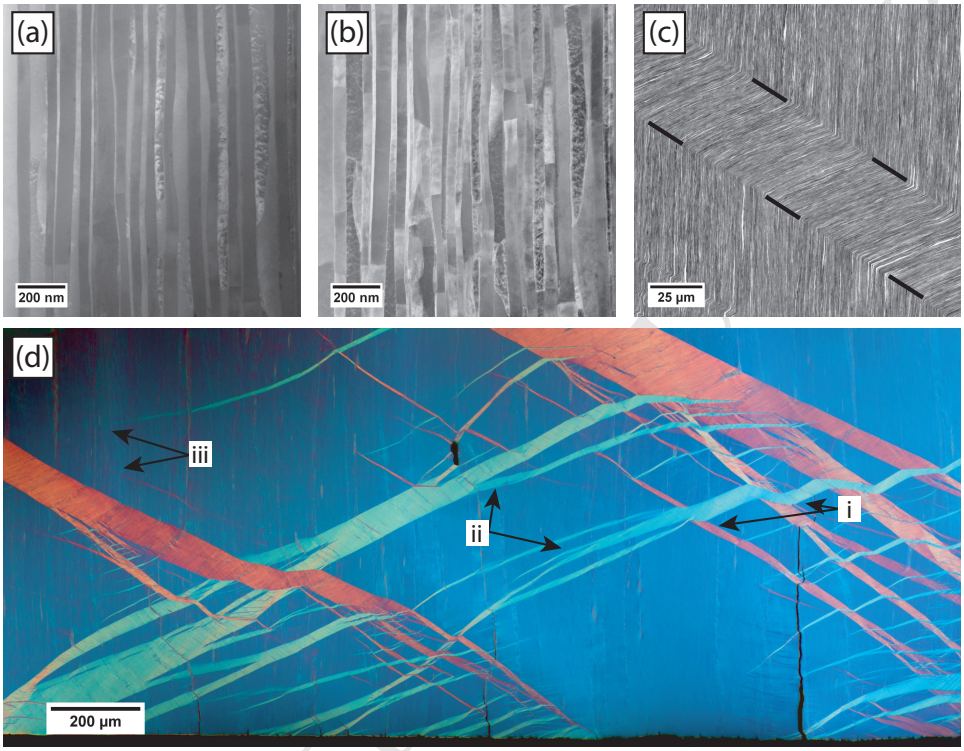

Figure 2: (a,b) STEM images of a 30 nm ARB Cu-Nb nanolaminate showing z-contrast where Cu layers are dark and Nb are lighter (a) and defect contrast where dislocations and grain boundaries are evident (b). (c) Backscatter SEM image of a single kink band in a 30 nm compression specimen with the kink band boundaries indicated with dashed lines, and (d) polarized light optical image of a complex network of kink bands in a 15 nm Cu-Nb compression specimen. Kink band intersections (i), bifurcations (ii), and terminations (iii) are evident, suggesting that kink bands formed sequentially via nucleation and propagation. Layer orientation in (a,b) and initial layer orientation/compression direction in (c,d) is vertical).

digital camera, Nikon AF Micro Nikkor 70-180 mm lens, fiber optic light source, and a half-silvered mirror for splitting the light source beam. This setup allowed for co-axial illumination of the polished specimens, yielding images containing good contrast between the dark toner speckles and reflective specimen surface. Images were acquired every 500 ms using the commercial acquisition software VIC-Snap 2009 (Correlated Solutions Inc.). While the full strain field should in theory require a two camera, 3D DIC set up, the strong anisotropy of the lamellar material combined with the early onset of kink band formation yielded a predominately plane strain deformation with the imaged surface of the specimen remaining within the focal plane of the imaging set up. The compression tests were interrupted once kink band propagation was complete (with the kink band spanning the width of the specimen).

2.3. DIC analysis

The images collected during compression testing were analyzed using VIC-2D 2009 software (Correlated Solutions Inc.). Based on the image size of 1908 x 2319 pixels and the speckle pattern (consisting of approximately 20 μm diameter speckles), a subset size of 49 x 49 pixels (102 x 102 μm) with a step size of 11 pixels (23 μm) was found to produce a good balance between correlation quality and strain resolution. A normalized squared differences criterion was used during correlation. While a local Gaussian decay kernel matrix is required in the software, the minimum kernel of 5 x 5 steps (55 x 55 pixels) was applied during the strain calculation [39]. The displacements and Lagrangian strain values were exported from VIC-2D, and all visualization and further analysis was conducted using MATLAB software.

Within the subset used to calculate strain, DIC treats the deformation as affine [39], and therefore significant care must be taken when using DIC on specimens that deform by heterogeneous and localized shear. If the subset used to calculate strain does not deform homogeneously and is instead sheared along a plane by a narrow kink band, correlation of the deformed state to the reference state is either impossible or very poor. The quality of correlation is represented by the 'sigma' value (one standard deviation confidence interval) calculated by the VIC-2D software. While the average sigma values for regions of the specimen that deformed uniformly were 0.012, indicating good correlation, higher values of sigma (~0.03) and uncorrelated subsets were found to correspond to the location of the kink band as it propagated across the sample. Thus the sigma value provided both a measure of the quality of the correlation and a convenient way to track the location of the kink band.

Calculated strain values for regions with a sigma value above 0.018 were discarded. This removed potentially unreliable strain measurements corresponding to the location of the kink band. However additional

cleanup of the strain data was needed due to the use of the Gaussian decay kernel during the strain calculation. While this filter reduces noise in the calculated strain values, it also increases the distance between two truly independent strain measurements. All calculated strain values in the area surrounding the kink band were removed by eroding the neighboring five strain measurements around any region containing a value of sigma greater than the threshold value (removing data within 122 μm of the kink band). All DIC strain maps are presented using the undeformed coordinates of each subset in order to allow calculated rather than interpolated strain values to be shown.

3. Results

3.1. Global stress-strain response and kink band initiation

Figure 3(b) shows the stress strain response of the compression specimen, with the strain calculated using the laser extensometer data. The results generally match the mechanical behavior expected based on prior tensile tests of the same material [38], although the slope of the linear segment is below the nominal Young's modulus as a result of compliance induced by the interfaces between the specimen and platens and the use of paste lubricant. The in situ images of the specimen surface were used to divide the stress strain curve into two regimes: one prior to the initiation of a visible kink band and labeled 'uniform compression' and one regime corresponding to and labeled 'kink band propagation.' The macroscopic stress strain curve does not display any sharp change of slope at the point of kink band initiation, making determination of these regimes dependent on in situ observations. Kink band propagation occurs initially under a rising load (from 1142 MPa to the maximum of 1205 MPa), however a sharp load drop (near the end of the stress strain curve) corresponds to the final propagation of the kink band across the specimen. Based on the behavior of other specimens and prior experiments [32], continued compression would be expected to induce kink band broadening at a near constant stress.

Compressive strain (ϵ_{yy}) maps of the imaged region of the specimen corresponding to points '1,' '2,' and '3' labeled on the stress strain curve are shown in Figure 3(c). Points 1 and 2 precede kink band formation while point 3 corresponds to the initiation of the kink band. As the specimen is loaded in the elastic range local strains appear fairly homogeneous although, due to the effects of friction at the specimens ends, a triangular constrained region near the specimen end and slight specimen barreling are expected. Elevated strain values are observed at the stress-concentrating specimen corners (evident in Figure 3(c3)), with the left hand corner showing higher local strains than the right hand corner. The overlaid displacement

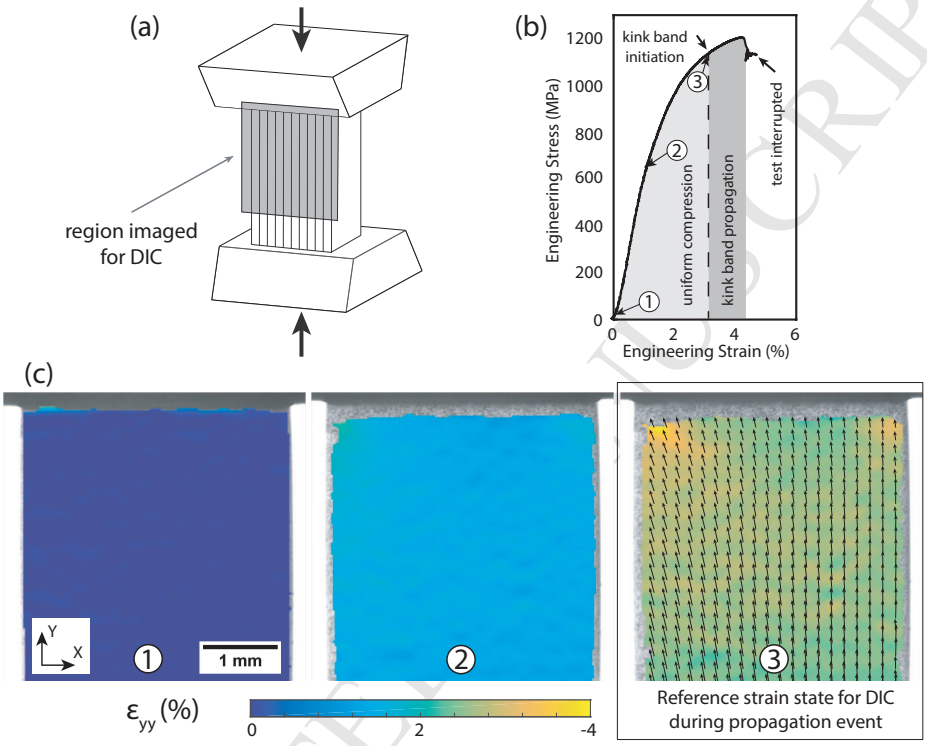

Figure 3: (a) Schematic of compression setup and DIC region, where the top platen remains stationary during the test. (b) Stress-strain curve annotated to show uniform compression regime, kink band initiation, and kink band propagation regime. Points 1, 2, and 3 prior to kink band initiation correspond to DIC strain maps (ϵ_{yy}) shown in (c). The displacement vector map overlay in (c3) indicates non-symmetric displacements which bias kink band formation to occur from the upper left corner. The strain distribution in part (c3) is taken to be the reference configuration for subsequent DIC analysis of the strains during kink band propagation, Figures 4 and 5.

vector map shows non-symmetric displacements which can be attributed to either non-uniform friction or a slight misalignment of the specimen. The asymmetric displacements are presumably responsible for kink band nucleation occurring at the left rather than right hand corner. Point '3' is taken to correspond to the beginning of kink band propagation, as this frame precedes the first frame in which a kink band can be clearly seen to extend from the top left corner. It is likely that the true initiation point occurs slightly earlier and would have been detected earlier had high magnification microscopy been conducted on that corner. As the focus of this study is kink band propagation and not initiation, it is reasonable to take point 3 as the beginning of kink band propagation. In order to distinguish small local strains during the subsequent kink band propagation, all DIC analysis of propagation uses the specimen state at point 3 as the reference state. This effectively zeros out the local strain values shown in Figure 3(c3) and allows the shape of the strain field in front of the propagating kink band to be shown clearly using the change in strain state from the reference configuration ($\Delta\epsilon_{xy}$ and $\Delta\epsilon_{yy}$). This referencing also minimizes the difference between the deformed and undeformed coordinate system, providing a more accurate representation of the strain fields.

3.2. Kink band propagation

Figures 4 and 5 show the stress strain curve, specimen image, and $\Delta\epsilon_{xy}$ and $\Delta\epsilon_{yy}$ strain maps during kink band propagation. The instantaneous stress, total specimen strain (from laser extensometer data), and time since initiation are shown on the stress strain curve. The kink band is evident as a dark band on the full resolution specimen images due to deformation induced surface relief, and an arrow is used to indicate the kink band tip location. The nominal angle of propagation and therefore kink band inclination angle (β) was ~27 degrees, although propagation across the last quarter of the specimen occurred at a more shallow angle of ~21 degrees.

The 2-D Lagrange strain tensor obtained from DIC has been transformed into a coordinate system in which the x-axis is aligned with the nominal direction of kink band propagation (a 27.5 degree rotation from the coordinate system used in Figure 3) and $\Delta\epsilon_{xy}$ lies parallel to the shearing action of the kink band. Continued uniform straining of the specimen during compression is evident in Figure 4, however the inhomogeneous strains adjacent to and in front of the kink band become clear as the kink band length increases. While some elevated local strains are present near the right hand corner, as expected due to the stress singularity at that location, no visible kink band is observed. The pronounced $\Delta\epsilon_{xy}$ strain field in front of the kink band shown in the bottom of Figure 4 extends across the entire specimen (millimeters ahead of the kink band tip), becoming more diffuse and lower in magnitude as the distance from the tip increases. The shear

strain field is aligned with the eventual propagation path.

During the second half of propagation, Figure 5, the strain fields in front of the kink band continue to increase in magnitude and spatial extent and the kink band propagation rate accelerates. No evidence of unloading is seen in the material behind the kink band tip during propagation. The kink band morphology during propagation is that of a very slender wedge (appearing crack-like), with the kink band width tapering from approximately ~30 microns near the initiation site to below 5 microns at the visible kink band tip. This is seen more clearly in Figure 6 which shows an image of the specimen taken one second before the kink band reaches the specimen edge. While the kink band taper is somewhat non-uniform, the nominal taper angle is ~0.5 degrees.

By identifying the kink band tip location, the strain fields obtained though DIC can be plotted in polar coordinates and compared to those of an inclined crack. Based on the inclination angle of the kink band (~27 degrees), a similarly inclined crack might be expected to have both a mode I and mode II component, however the mode I stress intensity factor would be negated by tractions arising from crack face closure. Therefore the kink band tip strain fields will be compared to those of a pure mode II crack. In addition to the elevated strains near the kink band tip (Figure 5(a,b)), significant homogeneous compression is observed during the early stages of kink band propagation (as seen from comparing Figure 4(a) to Figure 4(b)). Therefore it is expected that the experimentally observed kink band strain field consists of a superposition of a uniform far field strain and the strains associated with the stress singularity at the kink band tip.

Figure 7 compares the experimental kink band polar strain fields to those resulting from the combination of the analytical linear elastic fracture mechanics (LEFM) solution for a mode II crack and a small (0.4%) homogeneous compression. As with Figures 4 and 5, the large uniform strain prior to kink band initiation is not included in the strains presented in Figure 7. The magnitude of the small homogeneous strain that was included in the calculation was obtained from the difference between the experimentally measured 'far field' strain value at the lower end of the specimen (3.6 mm from the kink band tip) and the theoretical contribution of the mode II crack strains at the same location. It should be noted that the mode II crack stress intensity factor K_{II} was taken as a fit parameter, and therefore represents an 'effective' stress intensity factor that accounts for any bridging shear stress within the kink band. While recognizing that K_{11} was fit to the experimental data, the remarkably good agreement in the angular distributions of strain as well as the radial dependence of ϵ_{rr}, $\epsilon_{\theta\theta}$, and $\epsilon_{r\theta}$ shown in Figure 7 provides strong support for modeling kink band propagation using a fracture mechanics approach. Material anisotropy may be responsible for the small differences in the angular strain distributions between the kink band fields and the isotropic LEFM solution,

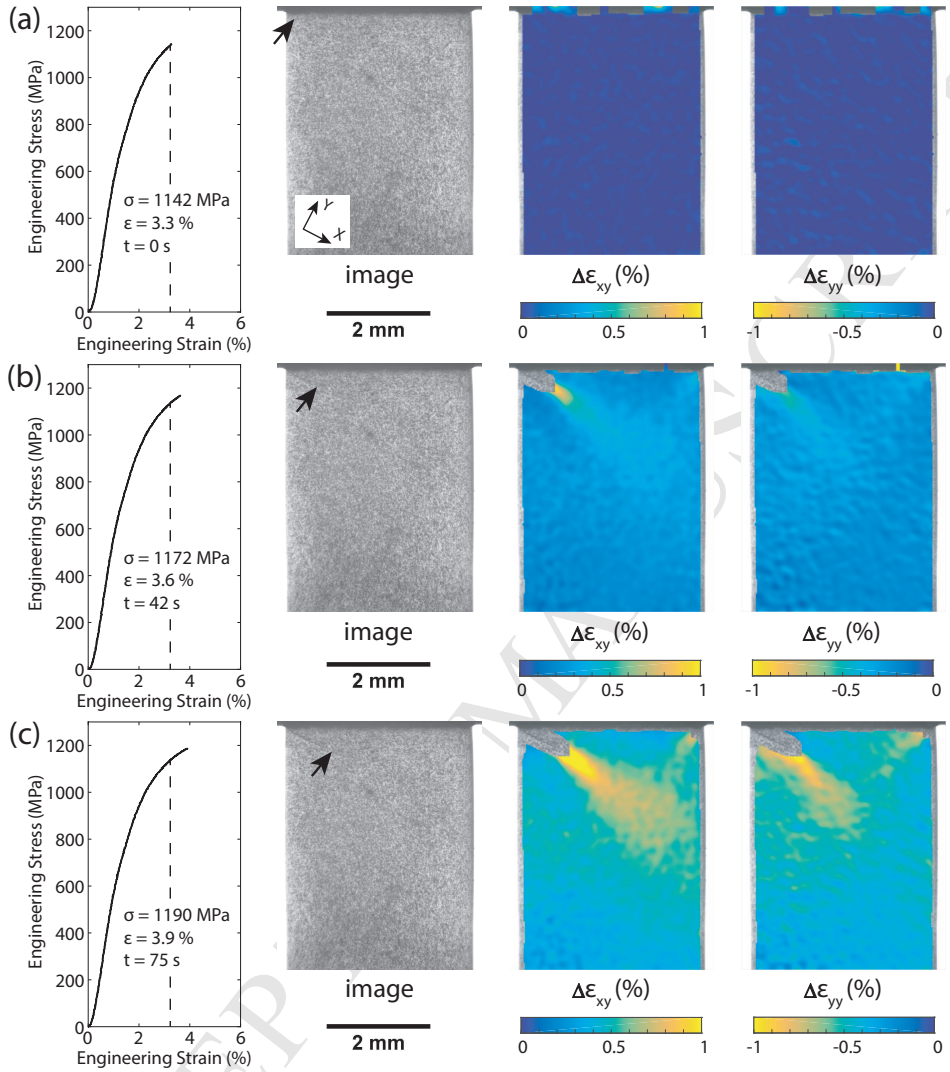

Figure 4: Kink band propagation, part 1: Stress-strain curve, in-situ image, $\Delta\epsilon_{xy}$ strain map, and $\Delta\epsilon_{yy}$ strain map during the initial stages of kink band propagation. The arrow indicates the tip of the kink band as determined from the full resolution optical images. Note that the coordinate system is rotated to align with the kink band propagation direction and that different scales are used for $\Delta\epsilon_{xy}$ and $\Delta\epsilon_{yy}$. All calculated strains are referenced to the state of the sample at the beginning of kink band propagation (dashed line on stress-strain curve) and therefore do not include the nearly homogeneous compression that occurred prior to kink band nucleation. Inset on the stress-strain diagram gives stress, total sample strain (ϵ), and time (t) relative to start of kink band propagation.

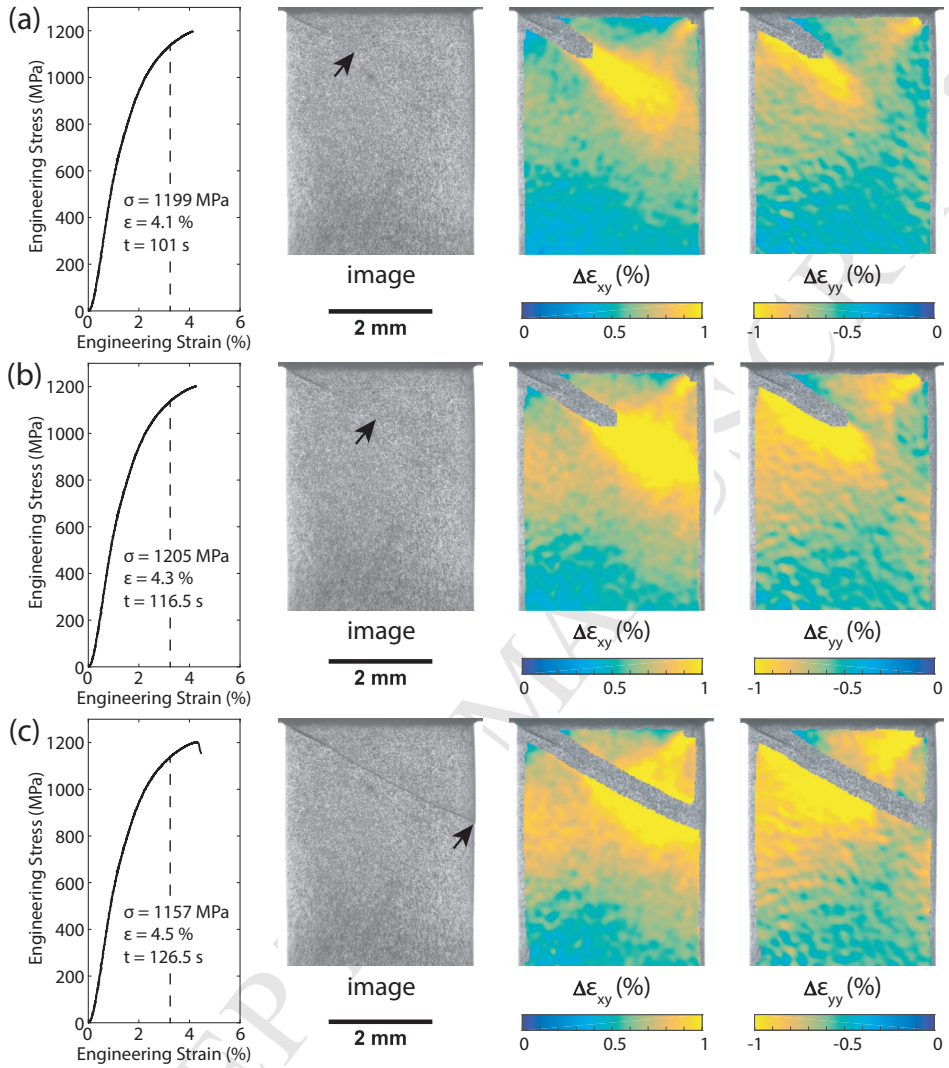

Figure 5: Kink band propagation, part 2: Stress-strain curve, in-situ image, $\Delta\epsilon_{xy}$ strain map, and $\Delta\epsilon_{yy}$ strain map during the later stages of kink band propagation. The arrow indicates the tip of the kink band as determined from the full resolution optical images. Note that the coordinate system is rotated to align with the kink band propagation direction and that different scales are used for $\Delta\epsilon_{xy}$ and $\Delta\epsilon_{yy}$. All calculated strains are referenced to the state of the sample at the beginning of kink band propagation (dashed line on stress-strain curve) and therefore do not include the nearly homogeneous compression that occurred prior to kink band nucleation. Inset on the stress-strain diagram gives stress, total sample strain (ϵ), and time (t) relative to start of kink band propagation.

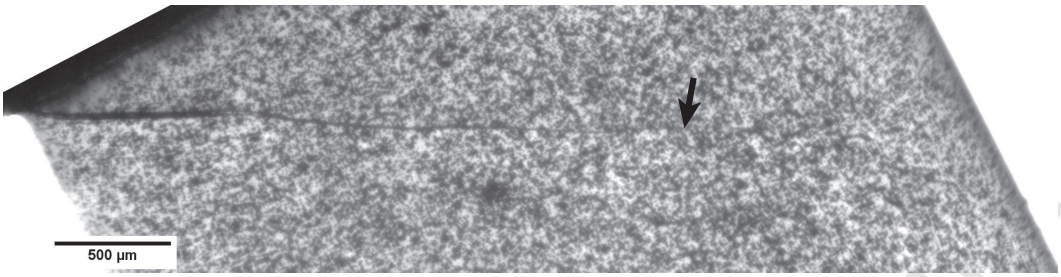

Figure 6: Full resolution image showing kink band extending from the specimen corner initiation site and terminating in the specimen (tip location is marked with an arrow). Image has been rotated 27.5 degrees. The kink band appears as a very slender wedge, tapering from approximately ~30 microns to below 5 microns over a length of 2.8 mm (a nominal wedge angle of ~0.5 degrees).

although the discrepancies and therefore potential effects of material anisotropy do not appear pronounced. Figure 8 provides a plot of the radial distribution of strains along the $\theta = 0$ and $\theta = -62.5$ degree lobes shown in Figure 7. These lobes are oriented away from the compression platen and are therefore least likely to be influenced by end constraints. The results in Figure 8 indicate generally good agreement between the kink band fields and the $r^{-\frac{1}{2}}$ singularity in the elastic crack tip solution.

The agreement between the mode II elastic crack tip fields and the experimental kink band strain fields may seem surprising given that at a macroscopic strain of ~4% these strain fields are expected to be fully plastic. While a more appropriate comparison would be that between the kink band and the Hutchinson, Rice, and Rosengren (HRR) plastic crack tip fields, analytical solutions for the mode II HRR field angular dependencies are, to the best of the authors' knowledge, unavailable. Therefore the analytical LEFM solutions are plotted, with the only modification being that volume preservation was enforced by setting the Poisson's ratio equal to 0.5. While the LEFM solution was used in place of the HRR solution, the difference between the two is slight when K_{II} is taken as a fit parameter. The HRR solutions show similar angular dependencies of strain and the HRR strain fields follow $r^{-\frac{n}{n+1}}$ [40], where n is the stress hardening exponent relating plastic strain (ϵ^p) to a material constant (α) and stress (σ): $\epsilon^p = \alpha\sigma^n$. For a near linear work hardening material ($n \approx 1$), the strain associated with the dominant singularity follows a relationship approximating $r^{-\frac{1}{2}}$. The small nonlinearity in the portion of the stress strain curve corresponding to kink propagation (Figure 3(b)) suggests that the strain associated with the dominant singularity would show an r dependence close to that obtained from LEFM (as observed in Figure 8). Thus, despite the strain fields at a macroscopic strain of ~4% being fully plastic, the subtle differences in r dependence between LEFM and HRR fields would not be distinguishable.

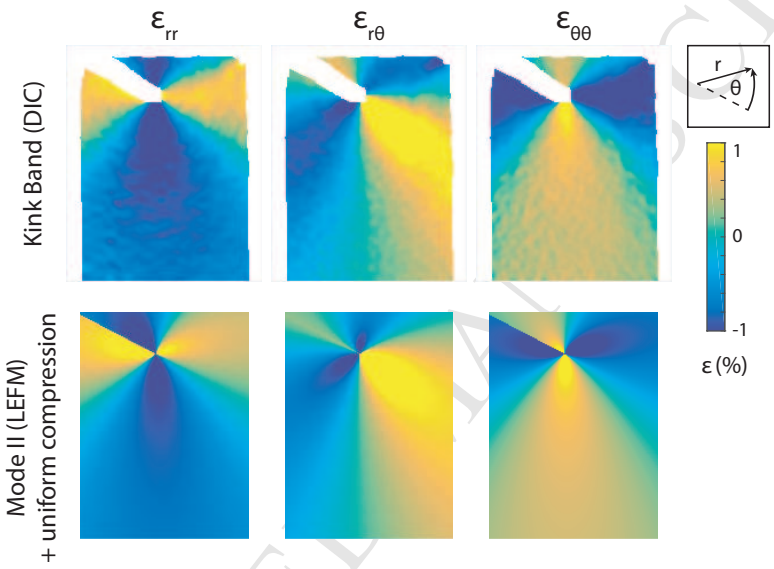

Figure 7: Polar strain fields during propagation are similar to those obtained from the superposition of the LEFM analytical solution for an inclined mode II crack and a uniform far field compressive strain. The polar coordinate system is rotated so that $\theta = 0$ is aligned with the kink band propagation direction. The elastic modulus was taken as 115 GPa (the average of Cu and Nb moduli), a Poisson's ratio of 0.5 was used, and the mode II stress intensity factor was fit to the experimental data, resulting in $K_{II} = 53$ MPa $\mathrm{m}^{1/2}$.

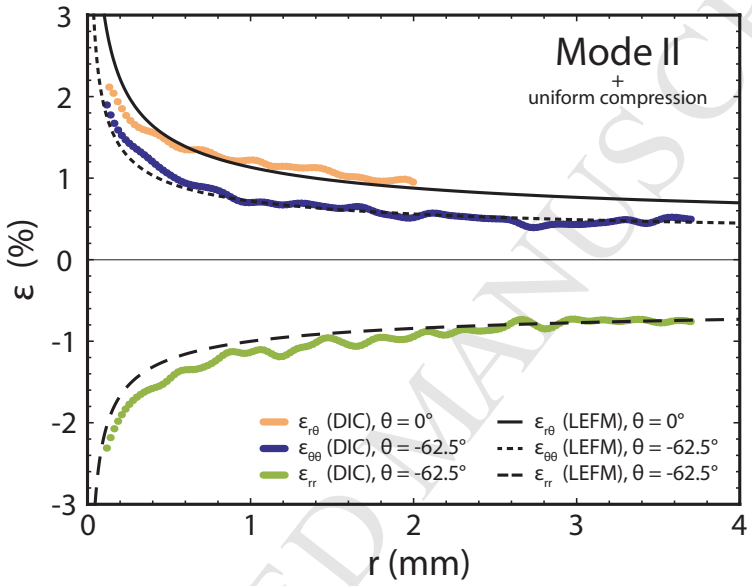

Figure 8: Radial dependence of kink band and mode II crack polar strain fields shown in Figure 7. ϵ_{rr} and $\epsilon_{\theta\theta}$ are plotted at $\theta = -62.5$ degrees while $\epsilon_{r\theta}$ is plotted along $\theta = 0$ degrees. These angles correspond to the two lobes in Figure 7 that are oriented away from the compression platens and are therefore least likely to be influenced by end constraints.

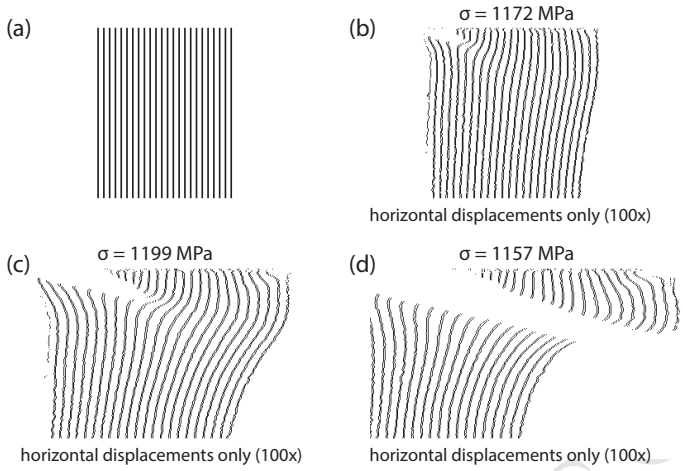

Figure 9: Exaggerated (100x) horizontal displacements are applied to an image containing vertical lines and representing the specimen (a). Images in (b), (c), and (d), correspond to Figure 4(b), Figure 5(a), and Figure 5(c) respectively. While vertical displacements are not included, these exaggerated representations point out features of the specimen distortion such as the reverse shear below the kink band in (b,c) that are mapped quantitatively in Figures 4 and 5.

While the strain field maps in Figures 4, 5, and 7 provide a quantitative description of the distortion of the specimen, a more intuitive picture is provided by exaggerating and applying the displacements obtained through DIC to a series of lines representing the layered sample. This approach is modeled on the work of Sun [26]. An image containing a series of vertical lines is generated with image dimensions matching the dimensions of the DIC displacement data array (see Figure 9(a)). Each pixel of the original image is displaced according to the DIC displacement data multiplied by a scaling factor (in the present case, 100). This large scaling factor, and therefore large exaggeration of the displacement, is employed to amplify the small strains observed during kink propagation. Due to this, it is only possible to apply the horizontal displacements; applying equally exaggerated vertical displacements would cause the image to collapse to nearly a line. Since only horizontal displacements are applied, angles are not reproduced faithfully and the small region around the kink band where displacement data are missing appears as if it were a material discontinuity. Nevertheless, Figure 9 provides an indication of the deformation pattern surrounding a propagating kink band and points out features such as the 'reverse shear' in the region below the kink band (Figure 9 (b,c)) that is present, but not as apparent, in the strain maps in Figures 4 and 5. The deformation of this region indicates that significant layer parallel shear occurs adjacent to the kink band flank to accommodate the kink band.

4. Discussion

The in situ observations presented in Figures 4 and 5 show that kink band formation in Cu-Nb laminates occurs by propagation of a kink band from a defect or stress concentration. This is in agreement with the literature for kink band formation in fiber composites, drawn polymers, and model systems such as compressed stacks of paper. [3, 4, 14, 18, 19, 41]. While much of the in-situ work reported in the literature has been conducted on specimens loaded in shear [4], combined shear and compression [18], or specimens containing a notch or artificial defect [3, 19, 42], Figures 4 and 5 indicate that stable kink band propagation can occur under a rising load during uniaxial compression of Cu-Nb laminates.

The strain fields ahead of and surrounding the propagating kink band are significant in magnitude and spatial extent: in Figure 5(b) a 1.5 mm^2 area of the strain field ahead of the kink band contains $\Delta\epsilon_{xy}$ values in excess of 1%. While the shear strain within the kink band is very large ($\gamma = 1.12$ given $\beta = 27.5$ degrees and $\phi = 2\beta$), the area of the kink band in Figure 5(b) is no greater than 0.03 mm^2. The work of deformation (Φ) is proportional to the area (A), plastic strain (ϵ_{ij}^p), and stress (σ_{ij}) of the material assuming plane strain fully plastic deformation (Equation 1).

$$\begin{aligned} \Phi &= \int \sigma_{ij}\epsilon_{ij}^p dV \\ &\propto \sigma_{ij}\epsilon_{ij}^p A \end{aligned} \tag{1}$$

Although simplistic, comparing the relative areas and shear strain magnitudes and assuming equal stresses inside and outside of the kink band indicates that the energy required to form the strain field extending in front of the kink band is approximately one half of the energy required to deform the material within the kink band. This evaluation almost certainly underestimates plastic dissipation in the strain field as the contributions of material sheared less than 1% and other strain components are neglected. While previous studies have examined the work contributions from deformations within a kink band and sought to explain the geometry of kink bands using energy minimization arguments [28, 29, 43], any prediction of total energy dissipation during kink band formation must include consideration of the deformation field in front of a propagating kink band.

Two distinct factors responsible for the local strain fields during kink band propagation can be identified: 1) compatibility between the wedge shaped kink band and non-kinked 'matrix' (accommodation strains) and 2) the stress concentration at the tip of a kink band terminating in a specimen. Accommodation strains around a wedge shaped kink band arise due to the variation in kink band width and continuity of layers

across the kink band. The homogeneous local shear strain in the material within a kink band with inclination β and rotation ϕ (Figure 1) is given by Equation 2.

$$\gamma = \sec^2(\phi - \beta) \tag{2}$$

The displacement of the layered structure across the kink band is given by the product of the width of the kink band and the shear strain within the kink band. The slightly wedge shaped kink band morphology shown in Figure 6 indicates a gradient in kink band width and therefore a gradient in displacements along the kink band boundary. This displacement gradient, combined with the observed layer continuity across kink bands [32], requires a corresponding displacement gradient in the non-kinked material adjacent to the band boundary. The necessity of an accommodation strain field surrounding a wedge shaped kink band has been pointed out in work on oriented polymers [44], and a close analogy is found in the strain field surrounding a deformation twin terminating in a single crystal [45]. Given the wedge shaped morphology of the propagating kink band (Figure 6) and the numerous non-parallel kink band boundaries observed post-test in compression specimens (Figure 2(d)), it appears that accommodation strain fields are commonly associated with kink bands in Cu-Nb laminates.

While accommodation strains are clearly required for a wedge shaped kink band, these strains are necessary in the material surrounding a propagating kink band regardless of the shape of the propagating band. They are an unavoidable result of compatibility between the kinked and non-kinked material when a kink band terminates in a specimen. Figure 10 shows several possibilities for the shape of a kink band propagating through a layered material. These schematics are drawn so that the layers outside of the kink band remain vertical, a simplifying representation that emphasizes the layer transverse component of the geometrically required strain field. Here it is assumed that the kink band need not grow in a self similar manner: the kink band 'tip zone' may have a different morphology than the portions of the kink band far removed from the tip. The uniform wedge shape, Figure 10(a), requires a linear displacement gradient at the boundary and leads to accommodation strains that are uniform along the length of the kink band. Figures 10(b), (c), and (d) show kink bands with parallel sides and various tip morphologies that result in accommodation strains present only near the tip zone. Varying the width of the kink band tip zone (Figure 10(b)) and varying the rotation ϕ in a kink band tip zone (Figure 10(c)) results in similar accommodation strains while a non-uniform wedge or elliptical kink band tip zone requires nonlinear displacement gradients at the boundary and results in non-uniform accommodation strains. Various morphologies of propagating kink bands have been reported in the literature: a self-similar wedge is consistent with the experimental observations of Robertson on kinks

in oriented polymers [4], a parallel sided band terminating in a wedge shaped tip zone was considered by Pertsev [46, 47], and a parallel sided band terminating in a zone of variable fiber rotation ϕ matches the observations of Vogler for kink bands in polymer matrix fiber composites [18]. Other experimental work points towards a combination of gradients in ϕ and gradients in kink band width at the tip zone of a kink band [3].

A clear difference in the distribution of accommodation strains is evident between a self-similar wedge (Figure 10(a)) and a band possessing parallel sides and a district tip zone (Figure 10(b), (c), and (d)). The question remains, however, of why one morphology should be preferred over another and whether the constitutive behavior of the material influences the morphology of a propagating kink band. Consider the two kink band morphologies shown in Figure 10(a) and (b) propagating through either an elastic or plastic specimen. The self-similar wedge shaped kink band (Figure 10(a)) has accommodation strains adjacent to the kink band. An incremental advance of the kink band (Figure 10(e)) subjects additional material now adjacent to the newly created kink band segment to the geometrically required accommodation strain. The material that was adjacent to the kink band boundary prior to its advance remains distorted. In contrast, the advance of a kink band with parallel sides and a wedge shaped tip zone (Figure 10(c)) requires both distortion of the material adjacent to the newly created kink band tip zone and a reversal of the accommodation strains in material that now lies next to the parallel boundary. This is illustrated in Figure 10(f). In the case of purely elastic accommodation strain fields, such a reversal of the accommodation strains behind the tip of the kink band would lower the strain energy in the material and should be preferred. If, however, the accommodation strain fields are predominantly plastic, such a reversal would be dissipative and require additional (redundant) plastic deformation. Thus a uniform wedge shape should be preferred when the accommodation strains are predominately plastic. This argument agrees with the observation that kink bands propagating through yielded Cu-Nb nanolaminates and polymers posses a fairly uniform wedge morphology [4], while kink bands propagating through fiber composites (in which the fibers remain elastic) tend to have parallel sided kink bands with a district tip zone [3, 18].

The second factor responsible for local strain fields during kink band propagation is the stress concentration that occurs at the tip of the kink band. The long, narrow, propagating kink band shown in Figure 6 has strong similarities to a mode II type shear crack and is found to have similar strain fields in front of the kink tip (Figure 7). Several investigators have proposed fracture mechanics based approaches to modeling kink band propagation. Moran and Shih [3] proposed modeling kink band propagation as growth of a predominantly mode II crack with bridging tractions through an anisotropic material, yet they did not have

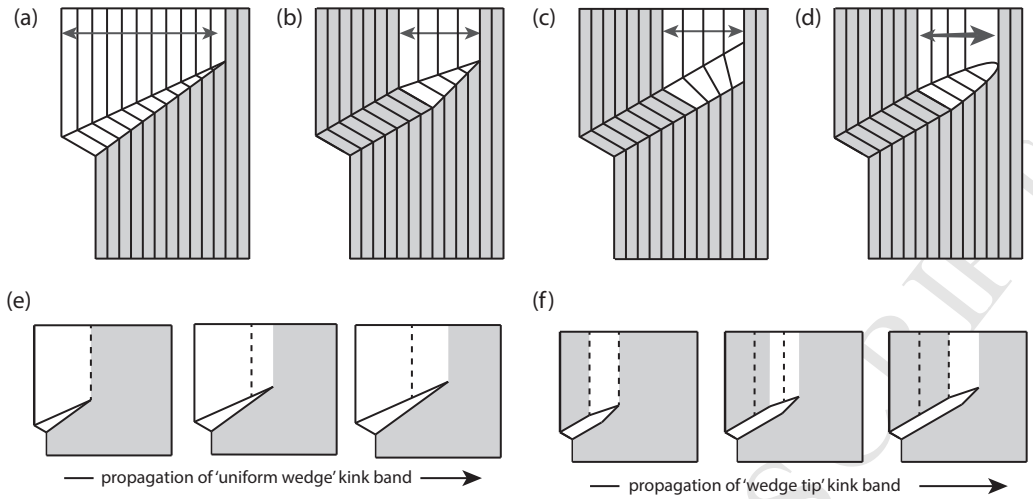

Figure 10: Schematic illustrating potential geometries for a kink band terminating in a specimen (a-d) and resultant accommodation strains. (e) and (f) show kink bands with either a uniform wedge shape (e) or a wedge shaped tip (f) advancing through the specimen. The shaded regions correspond to undistorted material and the dashed lines denote the original boundaries of the accommodation strain region.

the experimental fields in hand to motivate such a modeling effort. Bažant [48] proposed and conducted an analysis treating the kink band as a crack with a significant fracture process zone at the kink band tip. While no existing theoretical analysis accounting for material anisotropy, bridging tractions, and displacements prescribed by the kink band geometry is available to be compared with the experimental results shown in Figures 4, 5, and 7, the similarities to the mode II crack strain fields in Figure 7 are compelling. With the experimental kink band tip strain field data to serve as validation, the development of a fracture mechanics based approach to kink band propagation in metallic multilayers appears promising.

Both compatibility driven accommodation strains along the kink band flank and the extensive strain fields emanating from the kink band tip are expected to influence the direction of kink band propagation and therefore the kink band inclination angle β. The observed kink band inclination angle of $21 - 27$ degrees is far from the 45 degree angle expected from bifurcation analysis of plane strain shear localization in perfectly plastic isotropic materials [50], suggesting that these factors may have significant influence. In the case of the accommodation strains, the magnitude of the accommodation strain component parallel to the kink band boundary is set by the angle of the wedge shaped kink band and the shear strain within the kink band. The kink band inclination angle, β, determines how this strain component is oriented with respect

to the anisotropic material through which the kink band propagates. Various kink band inclination angles would result in different distributions of the accommodation strains in the surrounding anisotropic material and presumably different energy penalties associated with the accommodation strain fields. Likewise, the energy of the strain field in front of a propagating kink band should depend both on the constitutive behavior of the composite material and the orientation of the kink band. Attempts to predict why certain kink band inclination angles should be preferred without consideration of the details of kink band propagation neglect the effects of these extensive strain fields. Just as the prediction of crack propagation paths requires consideration of material anisotropy, it is likely that successful prediction of the kink band propagation angle requires consideration of the anisotropy and local deformation of the material surrounding the propagating kink band.

5. Conclusions

In this paper, digital image correlation was used to quantitatively assess the local strain fields surrounding a kink band propagating through a lamellar Cu-Nb composite with a layer thickness of 30 nm. The following conclusions are drawn from this work:

- Kink band formation in Cu-Nb laminates occurs via a nucleation and propagation sequence, in good agreement with the in situ observations of fiber composite kinking reported by Vogler [18].
- The wedge shaped morphology of the propagating kink band indicates the presence of an accommodation strain field adjacent to the kink band. These accommodation strains are required for any kink band with non-parallel band boundaries.
- A significant strain field resembling that expected for a mode II crack extends in front of the kink band during propagation. The size of this field is on the order of the kink band length, with the magnitude of distortion decreasing with distance from the kink band tip.
- While the strain level in the kink band tip strain field is approximately two orders of magnitude smaller than the strains within the kink band, the much larger volume of these strain field results in a significant contribution to the total work of kink band formation. The energy of the kink band tip strain field must be considered in any accurate calculation of energy dissipation during kinking.

Acknowledgments

The authors wish to acknowledge Michael Rossol (University of Illinois at Urbana-Champaign) and Chris Torbet (University of California Santa Barbara) for assistance with the digital image correlation setup. Helpful comments from Professor Samantha Daly (University of California Santa Barbara) are also greatly appreciated. T.J.N., I.J.B., N.A.M., J.T.A., and T.M.P. wish to acknowledge support by the UC office of the President, UC Lab Fees Research Program Award # 12-LR-238091. T.J.N. was supported by the Department of Defense through the National Defense Science & Engineering Graduate Fellowship (NDSEG) Program. This work was performed, in part, at the Center for Integrated Nanotechnologies, an Office of Science User Facility operated for the U.S. Department of Energy (DOE) Office of Science.

References

[1] A. S. Argon, Fracture of composites, Treatise on materials science and technology 1 (1972) 79–114.

[2] A. G. Evans, W. F. Adler, Kinking as a mode of structural degradation in carbon fiber composites, Acta Metall. 26 (1978) 725–738.

[3] P. M. Moran, C. F. Shih, Kink band propagation and broadening in ductile matrix fiber composites: Experiments and analysis, Int. J Solids Struct. 35 (1998) 1709–1722.

[4] R. E. Robertson, Formation of kink bands in oriented polymers, J. Polym. Sci: Part A-2: Polym. Phys. 7 (1969) 1315–1328.

[5] M. S. Paterson, L. E. Weiss, Experimental deformation and folding in phyllite, Geol. Soc. Am. Bull. 77 (1966) 343–374.

[6] T. B. Anderson, The relationship between kink–bands and shear fractures in the experimental deformation of slate, J. Geol. Soc. 130 (1974) 367–382.

[7] O. Mügge, Über translationen und verwandte erscheinungen in krystallen, Neu. Jahrb. Miner. Geol. Paäont. 1(1898) 71–159.

[8] L. Benabou, Predictions of compressive strength and kink band orientation for wood species, Mech. Mater. 42 (2010) 335–343.

[9] R. Menig, M. H. Meyers, M. A. Meyers, K. S. Vecchio, Quasi-static and dynamic mechanical response of *Haliotis rufescens* (abalone) shells, Acta Mater. 48 (2000) 2383–2398.

[10] E. Orowan, A type of plastic deformation new in metals, Nature 149 (1942) 463–464.

[11] M. W. Barsoum, T. Zhen, S. R. Kalidindi, M. Radovic, A. Murugaiah, Fully reversible, dislocation-based compressive deformation of Ti_3SiC_2 to 1 GPa, Nat. Mater. 2 (2003) 107–111.

[12] M. E. Manley, E. M. Schulson, Kinks and cracks in S1 ice under across-column compression, Philos. Mag. Lett. 75 (1997) 83–90.

[13] A. G. Crocker, J. S. Abell, The crystallography of deformation kinking, Philos. Mag. 33 (1976) 305–310.

[14] P. M. Moran, X. H. Liu, C. F. Shih, Kink band formation and band broadening in fiber composites under compressive loading, Acta Metall. Mater. 43 (1995) 2943–2958.

[15] J. B. Hess, C. S. Barrett, Structure and nature of kink bands in zinc, Trans. Am. Inst. Min. Met. Eng. (1949) 599–606.

[16] F. C. Frank, A. N. Stroh, On the theory of kinking, Proc. Phys. Soc. B 65 (1952) 811–821.

[17] I. Pane, H. M. Jensen, Plane strain bifurcation and its relation to kinkband formation in layered materials, Eur. J. Mech. A-Solids 23 (2004) 359–371.

[18] T. J. Vogler, S. Kyriakides, On the initiation and growth of kink bands in fiber composites: Part I. experiments, Int. J Solids Struct. 38 (2001) 2639–2651.

[19] A. M. Waas, C. D. Babcock, W. G. Knauss, An experimental study of compression failure of fibrous laminated composites in the presence of stress gradients, Int. J Solids Struct. 26 (1990) 1071–1098.

[20] N. A. Fleck, S. Sivashanker, M. P. F. Sutcliffe, Compressive failure of composites due to microbuckle growth, Eur. J. Mech. A-Solids 16 (1997) 65–82.

[21] M. P. F. Sutcliffe, N. A. Fleck, Microbuckle propagation in carbon fibre-epoxy composites, Acta Metall. Mater. 42 (1994) 2219–2231.

[22] J. L. Wind, A. M. Waas, H. M. Jensen, Initiation of failure at notches in unidirectional fiber composites, Compos. Struct. 122 (2015) 51–56.

[23] H. Koerber, J. Xavier, P. Camanho, High strain rate characterisation of unidirectional carbon-epoxy IM7-8552 in transverse compression and in-plane shear using digital image correlation, Mech. Mater. 42 (2010) 1004–1019.

[24] C. R. Chaplin, Compressive fracture in undirectional glass-reinforced plastics, J. Mater. Sci. 12 (1977) 347–352.

[25] F. Chiang, F. Jin, Q. Wang, N. Zhu, Speckle interferometry, in: IUTAM Symposium on Advanced Optical Methods and Applications in Solid Mechanics, Springer, pp. 177–190.

[26] W. Sun, A. P. Vassilopoulos, T. Keller, Experimental investigation of kink initiation and kink band formation in unidirectional glass fiber-reinforced polymer specimens, Compos. Struct. 130 (2015) 9–17.

[27] B. Budiansky, Micromechanics, Comput. Struct. 16 (1983) 3–12.

[28] M. A. Wadee, G. W. Hunt, M. A. Peletier, Kink band instability in layered structures, J. Mech. Phys. Solids 52 (2004) 1071–1091.

[29] R. A. E. Zidek, C. Völlmecke, Analytical studies on the imperfection sensitivity and on the kink band inclination angle of unidirectional fiber composites, Comp. Part A 64 (2014) 177–184.

[30] N. A. Fleck, B. Budiansky, Compressive failure of fibre composites due to microbuckling, in: Inelastic deformation of composite materials, Springer, 1991, pp. 235–273.

[31] B. Budiansky, N. A. Fleck, J. C. Amazigo, On kink-band propagation in fiber composites, J. Mech. Phys. Solids 46 (1998) 1637–1653.

[32] T. Nizolek, N. A. Mara, I. J. Beyerlein, J. T. Avallone, T. M. Pollock, Enhanced plasticity via kinking in cubic metallic nanolaminates, Adv. Eng. Mater. 17 (2015) 781–785.

[33] T. Nizolek, N. A. Mara, I. J. Beyerlein, J. T. Avallone, J. E. Scott, T. M. Pollock, Processing and deformation behavior of bulk Cu–Nb nanolaminates, Metall. Micro. Anal. 3 (2014) 470–476.

[34] J. S. Carpenter, R. J. McCabe, S. J. Zheng, T. A. Wynn, N. A. Mara, I. J. Beyerlein, Processing parameter influence on texture and microstructural evolution in Cu-Nb multilayer composites fabricated via accumulative roll bonding, Metall. Mater. Trans. A 45 (2014) 2192–2208.

[35] I. J. Beyerlein, N. A. Mara, J. S. Carpenter, T. Nizolek, W. M. Mook, T. A. Wynn, R. J. McCabe, J. R. Mayeur, K. Kang, S. Zheng, J. Wang, T. M. Pollock, Interface-driven microstructure development and ultra high strength of bulk nanostructured Cu-Nb multilayers fabricated by severe plastic deformation, J. Mater. Res. 28 (2013) 1799–1812.

[36] J. S. Carpenter, S. C. Vogel, J. E. LeDonne, D. L. Hammon, I. J. Beyerlein, N. A. Mara, Bulk texture evolution of Cu-Nb nanolamellar composites during accumulative roll bonding, Acta Mater. 60 (2012) 1576–1586.

[37] I. J. Beyerlein, N. A. Mara, J. Wang, J. S. Carpenter, S. J. Zheng, W. Z. Han, R. F. Zhang, K. Kang, T. Nizolek, T. M. Pollock, Structure-property-functionality of bimetal interfaces, JOM 64 (2012) 1192–1207.

[38] T. Nizolek, I. J. Beyerlein, N. A. Mara, J. T. Avallone, T. M. Pollock, Tensile behavior and flow stress anisotropy of accumulative roll bonded Cu-Nb nanolaminates, Appl. Phys. Lett. 108 (2016) 051903.

[39] M. A. Sutton, J. J. Orteu, H. Schreier, Image correlation for shape, motion and deformation measurements: basic concepts, theory and applications, Springer Science & Business Media, 2009.

[40] J. Hutchinson, Plastic stress and strain fields at a crack tip, J. Mech. Phys. Solids 16 (1968) 337–342.

[41] L. E. Weiss, Flexural slip folding of foliated model materials, in: A. Baer, D. Norris (Eds.), Proc. Conference on Research in Tectonics (Kink bands and brittle deformation), pp. 294–333.

[42] T. Vogler, S. Kyriakides, Initiation and axial propagation of kink bands in fiber composites, Acta Mater. 45 (1997) 2443–2454.

[43] M. A. Wadee, C. Völlmecke, J. F. Haley, S. Yiatros, Geometric modelling of kink banding in laminated structures, Phil. Trans. R. Soc. A 370 (2012) 1827–1849.

[44] D. Martin, E. Thomas, Micromechanisms of kinking in rigid-rod polymer fibres, J. Mater. Sci. 26 (1991) 5171–5183.

[45] J. W. Christian, S. Mahajan, Deformation twinning, Prog. Mater Sci. 39 (1995) 1–157.

[46] N. A. Pertsev, A. E. Romanov, Instability of front profiles of kink bands in oriented polymers, Mech. Compos. Mater. 19 (1984) 565–570.

[47] N. Pertsev, V. Marikhin, L. Myasnikova, Z. Pelzbauer, Incomplete kink bands in fully oriented high-density polyethylene, Polym. Sci. (USSR) 27 (1985) 1611–1620.

[48] Z. P. Bažant, J.-J. H. Kim, I. M. Daniel, E. Becq-Giraudon, G. Zi, Size effect on compression strength of fiber composites failing by kink band propagation, in: Fracture Scaling, Springer, 1999, pp. 103–141.

[49] B. L. Hansen, J. S. Carpenter, S. D. Sintay, C. A. Bronkhorst, R. J. McCabe, J. R. Mayeur, H. M. Mourad,I. J. Beyerlein, N. A. Mara, S. R. Chen, G. T. Gray, Modeling the texture evolution of Cu/Nb layered composites during rolling, Int. J. Plast. 49 (2013) 71–84.

[50] J. W. Hutchinson, V. Tvergaard, Shear band formation in plane strain, Int. J Solids Struct. 17 (1981) 451–470.